Sedimentary Geology 429 (2022) 106079

Contents lists available at ScienceDirect

Sedimentary Geology

journal homepage: www.elsevier.com/locate/sedgeo

Temperature regimes during formation of Miocene island dolostones as determined by clumped isotope thermometry: Xisha Islands, South China Sea

Rui Wang [a], Yang Xiao [a], Kefu Yu [a,b,*], Brian Jones [c], Lü Wu [a], Feng Liang [d,e], Yang Yang [a], Biao Chang [f,g]

[a] Guangxi Laboratory on the Study of Coral Reefs in the South China Sea, Coral Reef Research Center of China, School of Marine Sciences, Guangxi University, Nanning 530004, China
[b] Southern Marine Science and Engineering Guangdong Laboratory, Zhuhai 519080, China
[c] Department of Earth and Atmospheric Sciences, University of Alberta, Edmonton, Alberta T5R 3C8, Canada
[d] Key Laboratory of Carbonate Reservoirs, CNPC, Hangzhou 310023, China
[e] PetroChina Hangzhou Research Institute of Geology, Hangzhou 310023, China
[f] State Key Laboratory of Biogeology and Environmental Geology, School of Earth Science, China University of Geosciences, Wuhan 430074, China
[g] State Key Laboratory of Geological Processes and Mineral Resources, China University of Geosciences, Wuhan 430074, China

ARTICLE INFO

Article history:
Received 3 November 2021
Received in revised form 29 December 2021
Accepted 30 December 2021
Available online 7 January 2022

Editor: Dr. Jasper Knight

Keywords:
Carbonate clumped isotopes
Temperature
Dolostones
Cenozoic
Xisha Islands

ABSTRACT

Carbonate clumped isotope thermometry is a relatively new type of analysis that has been used to obtain a better understanding of the temperature and salinity of the water that mediated the development of dolostones in the Cenozoic successions of isolated oceanic islands. There is, however, still some uncertainty about the factors that could modify the clumped isotopes even in shallow burial conditions and thereby affect the temperatures and salinities derived from them. Here, focus is placed on a 210.5 m thick succession of Miocene dolostones that is found on the Xisha islands in the South China Sea that have experienced rapid subsidence since the Early Miocene. These dolostones are typically formed of crystals that have a "dirty" core that is encased by a clear outer rim. The formation of the "dirty cores", the primary replacement dolomite, was probably mediated by normal seawater in near-surface conditions, whereas the later cements formed at higher temperatures from slightly evaporated seawater. Given that it is impossible to separate the "dirty cores" from the clear rimes for analytical purposes, it must be recognized that the clumped isotopes and other geochemical data (e.g., $\delta^{18}O$, $^{87}Sr/^{86}Sr$) are averages of these two types of dolomite. This also means that the development of dolomite in these dolostones involved two successive stages of dolomite development that was probably related to sea-level cycles. Despite these issues, clumped isotope thermometry can still provide valuable temperature and salinity information for understanding the dolomitization processes that led to the development of island dolostones.

1. Introduction

The "dolomite problem", which refers to the enigmatic origin of dolomite in natural environments, has existed for more than two centuries despite the extensive research that has focused on this issue (Land, 1985; Warren, 2000; Machel, 2004). Virtually every proposed dolomitization model invoked to explain the formation of dolostones involves debate about the temperature and salinity of the fluids responsible for dolomitization (Budd, 1997; Warren, 2000; Machel, 2004). Most of the approaches used to determine these parameters remain problematic with the results open to debate. In recent years, carbonate clumped isotope thermometry (or 'Δ_{47} thermometry') (Ghosh et al., 2006; Schauble et al., 2006, Eiler, 2007, 2011), which is based on the temperature-dependent formation of $^{13}C^{18}O^{16}O_2^{2-}$ ion groups in solid carbonate minerals, has been used to determine the formation temperature (Chang et al., 2020), the $\delta^{18}O_{water}$, and the salinity of the fluids that mediated the formation of ancient dolostones (Lukoczki et al., 2020).

Cenozoic "island dolostones", found on many isolated oceanic islands throughout the world, have been considered natural laboratories for resolution of the "dolomite problem" because the dolostones are <12 Ma old, have not been deeply buried (<1 km), and appear to have formed under conditions akin to those of their modern-day settings (e.g., Budd, 1997; Ren and Jones, 2018; Wang et al., 2019). In recent years, clumped isotopes have been applied to some of these island dolostones in an effort to constrain the temperature and salinity

* Corresponding author at: Guangxi Laboratory on the Study of Coral Reefs in the South China Sea, Coral Reef Research Center of China, School of Marine Sciences, Guangxi University, Nanning 530004, China.
E-mail address: kefuyu@scsio.ac.cn (K. Yu).

https://doi.org/10.1016/j.sedgeo.2021.106079
0037-0738/

($\delta^{18}O_{water}$) of the formative fluids. Notable examples include the studies of the Bahamian Platform in the North Atlantic (Winkelstern and Lohmann, 2016; Murray and Swart, 2017), Meiji Reef in the South China Sea (Guo et al., 2021), and the Marion Plateau in northeast Australia (Veillard et al., 2019). In some cases, however, the clumped isotopes of these island dolostones may have been partly reset by recrystallization and therefore no longer reflect the original formation temperatures. For example, available evidence indicates that the clumped isotopes derived from the Miocene dolostones of the Marion Plateau may have been influenced by recrystallization (Veillard et al., 2019) even though the sequence had not been deeply buried (<1 km) and was not affected by high temperature (>50 °C) conditions. Based on the analysis of a 4500 m thick succession from Andros Island, Bahama Platform, Winkelstern and Lohmann (2016) argued that the clumped isotopes of the limestones and dolostones at depths of <1.3 km were not affected by recrystallization. Similarly, dolostones from the Bahamian Platform (Murray and Swart, 2017; Murray et al., 2021) and from well NK-1 on Meiji reef in the South China Sea (Guo et al., 2021) were also considered unaffected by diagenetic alteration. Nevertheless, it is clear that diagenetic alteration of dolostones may also lead to modification of the clumped isotopes and, hence, affect any temperatures and salinity values derived from them.

Herein, clumped isotopes are used to evaluate the island dolostones of the Huangliu Formation in well CK-2 (928.75 m deep) that was drilled on Chenhang Island, which is part of the Xisha Islands, South China Sea (Fig. 1A, B). Attention is focused on these mostly pure dolostones (average dolomite content >98%) that are now found 308.5 to 519 m below modern sea-level (bsl) (Fig. 1C). These dolostones are texturally and compositionally similar (e.g., composed mainly of Ca-rich dolomite) to many Cenozoic island dolostones found on islands throughout the Caribbean Sea and the Pacific Ocean (Ren and Jones, 2018; Wang et al., 2018, 2019). In this study, the clumped isotopes of the dolostones from the Huangliu Formation are considered along with detailed petrological, mineralogical and geochemical data to: (1) constrain the temperature and salinity of the fluid that mediated dolomitization, (2) evaluate the possible effects of diagenetic alteration on the clumped isotopes, and (3) evaluate the dolomitization models that are viable given the information derived from the clumped isotopes. Critically, the results show that even under conditions of early shallow-buried dolomitization, the clumped isotope thermometry of dolostones may be affected by the later formed dolomite cements that are present in most of the dolostones. Nevertheless, careful interpretation of the clumped isotopes can still provide valuable data for constraining the conditions under which dolomitization took place.

2. Geological setting

The Xisha Islands (also known as the Paracel Islands), occupying an area of ~500,000 km^2, are located on an isolated platform in the northern part of the South China Sea and surrounded by water that is more than 1000 m deep (Fig. 1A, B). Data from three deep wells (XY-1, XK-1, and CK-2) show that the Xisha Platform was initiated during the early Miocene, ~20 Ma ago (Yi et al., 2018; Fan et al., 2020). Since then, the Jurassic and/or Cretaceous metamorphic/volcanic basement rocks of the Xisha platform have subsided rapidly and it is now covered by a ~1200 m thick succession of carbonate sediments (Wu et al., 2014;

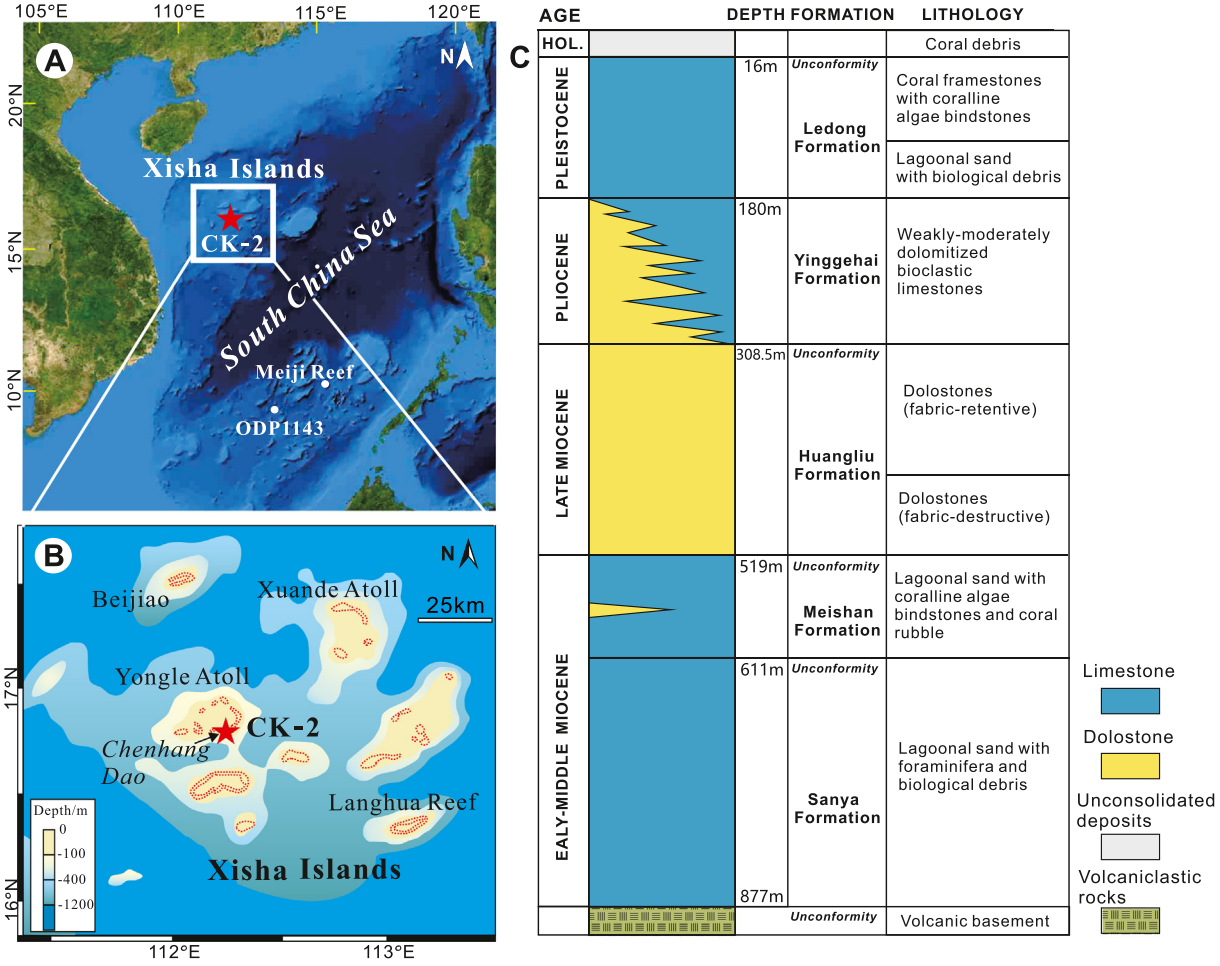

Fig. 1. (A) Location of Xisha Islands and wells in the South China Sea. (B) Location of well CK-2. (C) Stratigraphic succession on Xisha Platform. (Modified from Wang et al. (2021).)

Zhu et al., 2017; Zhang et al., 2020). Today, the Xisha Islands comprise numerous islands, reefs and shoals that have their surfaces near modern sea-level. Annual rainfall is 1300 to 2000 mm and annual average surface seawater temperature is 26.8 °C (22 to 30 °C range) with a near-surface salinity of 33.1 to 34.2‰ (Shao et al., 2017a, 2017b).

Unconformities in the carbonate succession on the Xisha Islands divide the succession, in ascending order, into the Sanya Formation, Meishan Formation, Huangliu Formation, Yinggehai Formation, and Ledong Formation (Fig. 1C) (Zhao, 2010; Wu et al., 2014; Shao et al., 2017a, 2017b). The Huangliu Formation, >200 m thick and composed mostly of finely crystalline dolomites, contrasts with the other formations that are formed largely of limestone or partly dolomitized limestone. Available evidence indicates that the Huangliu Formation is late Miocene in age (Zhao, 2010; Shao et al., 2017a, 2017b; Wang et al., 2018). During deposition of the sediments that now form this formation, the platforms began to backstep in response to relative sea-level rise and only a few isolated carbonate buildups persisted (Wu et al., 2014). The sediments that now form the Huangliu Formation were deposited in shallow water reef flat and lagoonal settings during the late Miocene (Wang et al., 2018, 2021).

3. Methods

Well CK-2 was drilled and cored to a depth of 928.75 m below sea level (bsl) in 2013 by the Wuhan Institute of Geotechnical Mechanics and the South China Sea Institute of Oceanology (Chinese Academy of Sciences) with a recovery of >70%. For the dolostones of the Huangliu Formation, found 308.5 to 519 m (bsl), the recovery rate was >80% (Wang et al., 2018).

After detailed documentation and description of the core from the Huangliu Formation, 126 samples (1 to 3 m intervals) were selected for thin-section analyses in order to establish their petrological characteristics. In addition, thick thin-sections (~50 μm thick) were made for analysis of (1) fluid inclusions (n = 12) and (2) backscatter electron imaging (n = 24). Fluid inclusions, found under the microscope, were analyzed using a Linkam thms-600 a heating and cooling stage at Xi'an Petroleum University, China. The starting heating/cooling temperature was at room temperature (20 °C) and the heating/cooling rate was controlled within 5–10 °C/min. Backscatter electron (BSE) images and spot analyses were obtained using a JEOL 8230 electron microprobe (EMP), located at Guangxi University (China), that was operated with a 10 kV accelerating voltage with a 15 nA beam current.

Lithological samples (n = 103), obtained by micro drilling of the core at ~2 m intervals, were washed in distilled water, dried in an oven at ~40 °C, and ground into a powder (<74 μm) using an agate mortar and pestle. Dolomite stoichiometry, oxygen isotopes, and elemental (Sr, Mn) analyses of these samples, first reported in Wang et al. (2018) were undertaken at Guangxi University, China. Dolomite stoichiometry (mol% $CaCO_3$; hereafter referred as %Ca) was measured and reported following the protocol of Jones et al. (2001). The oxygen isotopes are reported in standard delta (δ) notation in per mil (‰) relative to Vienna Peedee belemnite (VPDB) with a standard deviation of 0.08% for $\delta^{18}O$. $\delta^{18}O$ fractionation, caused by acid digestion of the dolomite, was corrected using the fractionation factor of Rosenbaum and Sheppard (1986). Elemental (Sr, Mn) analyses were obtained at Guangxi University using inductively coupled plasma mass spectrometry (ICP-MS). The $^{87}Sr/^{86}Sr$ ratios of 27 samples were determined at the University of Queensland using a VG Sector-54 thermal ionization mass spectrometer and corrected to the NIST-987 value of 0.710248. The McArthur et al. (2001) LOWESS lookup curve was used to determine the relative ages. These supplement the 25 $^{87}Sr/^{86}Sr$ values given in Wang et al. (2018).

Twenty-two powdered samples (~10 m interval) with Mn/Sr < 0.2 (average value of Mn/Sr for Huangliu dolostones is 0.2) were selected for clumped isotope analysis at the China University of Geosciences at Wuhan using the same conditions (e.g., 90 °C acid reaction temperature) reported by Chang et al. (2020). Each sample was measured two to five times, and each run was tested by eight acquisition cycles. The results, reported as Δ_{47} in per mil (‰) (Ghosh et al., 2006), reflect the overabundance of $^{13}C^{18}O^{16}O$ relative to the stochastic distribution (Eiler, 2007). The acquired raw Δ_{47} values were transferred into an absolute reference frame (ARF), which was calculated using CO_2 reference gasses equilibrated at 10, 25, 50, and 1000 °C (Dennis et al., 2011). Typical sample precision of the Δ_{47} data based on replicate measurements of our dolomite samples is 0.010‰ (1 SE). Standard oxygen isotopes ($\delta^{18}O$) were also acquired in this process so that they could be compared to those obtained using standard isotope techniques from Wang et al. (2018).

Herein, the Δ_{47}-T calibrations recommended by Bonifacie et al. (2017) (90 °C acid reaction temperature) and by Müller et al. (2019) (70 °C acid reaction temperature) for dolomite and Petersen et al. (2019) (25 °C acid reaction temperature) and Anderson et al. (2021) for carbonate minerals are used to constrain the relationship between dolomite formation temperature (T) and clumped isotope values (Δ_{47}):

(1) $\Delta_{47CDES90} = 0.0428\ (\pm0.0033) * (10^6 / T^2) + 0.1174\ (\pm0.0248)$ ($r^2 = 0.997$) (Bonifacie et al., 2017);
(2) $\Delta_{47CDES70} = 0.0428\ (\pm0.0020) * (10^6 / T^2) + 0.1481\ (\pm0.0160)$ ($r^2 = 0.864$) (Müller et al., 2019);
(3) $\Delta_{47\ CDES25} = 0.0383 * (10^6 / T^2) + 0.258$ ($r^2 = 0.864$) (Petersen et al., 2019);
(4) $\Delta_{47\ (I\text{-}CDES90)} = 0.0390(\pm0.0004) * (10^6 / T^2) + 0.153\ (\pm0.004)$ ($r^2 = 0.97$) (Anderson et al., 2021).

We also used the $10^3 \ln\alpha - T$ equations from Matthews and Katz (1977), Vasconcelos et al. (2005), Horita (2014), and Müller et al. (2019), respectively, to constrain the $\delta^{18}O_{water}$ (‰; VSMOW: Vienna Standard Mean Ocean Water) using $T(\Delta_{47})$ (calculated temperature derived from Δ_{47}) and $\delta^{18}O_{dolomite}$:

(5) $10^3 \ln \alpha_{dolomite\text{-}water} = 3.06 * (10^6 / T^2) - 3.24$ (Matthews and Katz, 1977);
(6) $10^3 \ln \alpha_{dolomite\text{-}water} = 2.73 * (10^6 / T^2) + 0.26$ (Vasconcelos et al., 2005);
(7) $10^3 \ln \alpha_{dolomite\text{-}water} = 3.14(\pm0.022) * (10^6/T^2) - 3.14\ (\pm0.11)$ (Horita, 2014);
(8) $10^3 \ln \alpha_{dolomite\text{-}water} = 2.9923\ (\pm0.0557) * (10^6/T^2) - 2.3592$ (±0.4116) ($r^2 = 0.9164$) (Müller et al., 2019).

In the above formulas, $\alpha_{dolomite\text{-}water} = (\delta^{18}O_{dolomite} + 1000) / (\delta^{18}O_{water} + 1000)$. The $\delta^{18}O_{dolomite}$ is in VSMOW. The $\delta^{18}O_{dolomite}$ (VPDB) is transferred into $\delta^{18}O_{dolomite}$ (VSMOW) by using Kim et al. (2015): $\delta^{18}O_{dolomite}$ (VSMOW) = 1.03092 * $\delta^{18}O_{dolomite}$ (VPDB) + 30.92.

4. Results

4.1. Petrology

The formation is divided into four unconformity-bounded units (units 1 to 4) (Fig. 2A) based on their petrologic and geochemical characteristics. Units 2 to 4, which form the upper part of the formation (308.5 to 434.5 m bsl), are composed of gray fabric-retentive rudstones, bindstones, packstones, and wackstones (Fig. 2B) with dolomite crystals that are mostly <60 μm long. Red algae, *Halimeda*, and foraminifer fragments are most common in these rocks (Wang et al., 2018). In contrast, unit 1, which constitutes the lower part of the formation (434.5 to 519 m bsl), is formed of tan, fabric-destructive dolostones with crystals 10 to 140 μm long (Fig. 2A). The euhedral to subhedral dolomite crystals of the Huangliu Formation typically have inclusion-rich dark (dirty) cores encased by clear rims (1–10 μm thick) (Fig. 3A, B). Under Cathodoluminescene (CL) images, the "dirty" cores generally present bright red, while the clear rims are dull red (Wang et al., 2018; their Fig. 7).

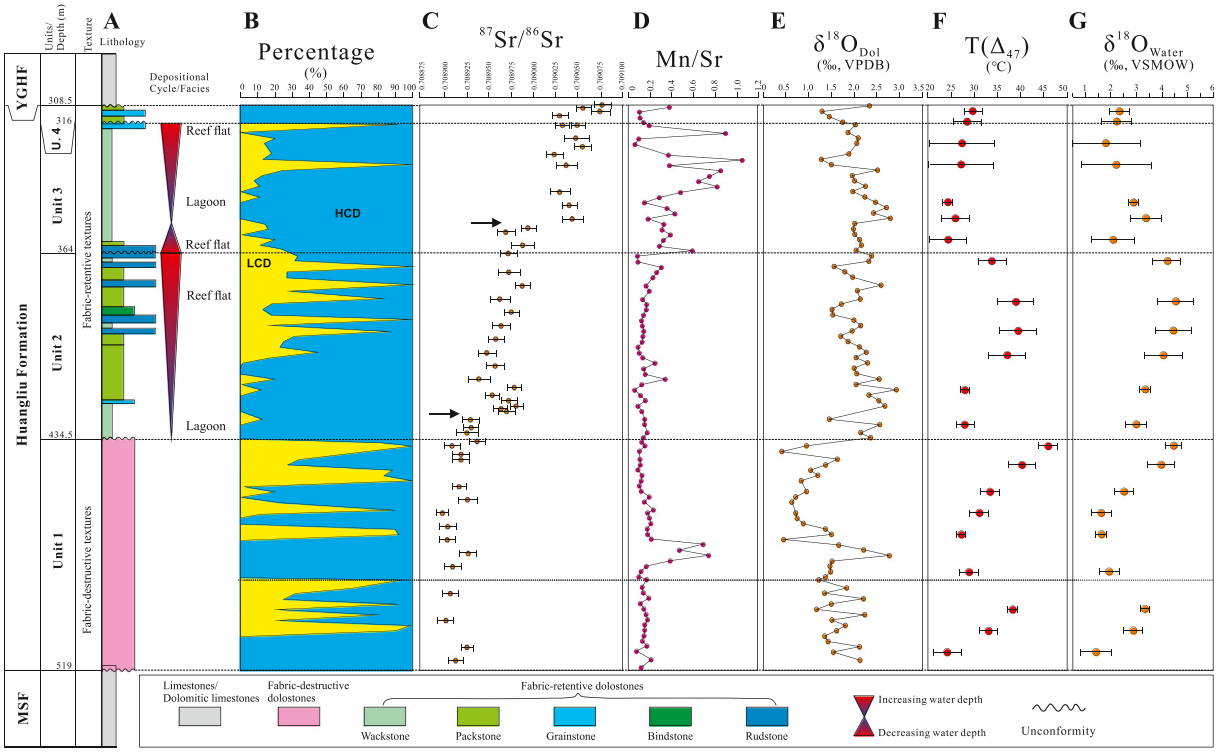

Fig. 2. Lithology, facies, and geochemical characteristics of dolostones in the Huangliu Formation from well CK-2, Xisha Islands. MSF, Meishan Formation; YGHF, Yinggehai Formation. (A) Lithological succession and succession of depositional facies. (B) Stratigraphic variations in distribution of low-Ca dolomite (LCD, <55%Ca) and high-Ca dolomite (HCD, >55%Ca), from Wang et al. (2021, their Fig. 2). (D) $^{87}Sr/^{86}Sr$ ratios. Note the two obvious "jumps" in $^{87}Sr/^{86}Sr$ values (black arrows). (E) Mn/Sr values. (F) $\delta^{18}O_{dolostone}$ values (‰, VPDB). (G) Calculated formation temperature ($T(\Delta_{47})$, °C) derived from clumped isotopes (Δ_{47}) using the Bonifacie et al. (2017) Δ_{47}-T calibration. (H) Calculated $\delta^{18}O_{water}$ values (‰; VSWOM) using the $10^3 ln\alpha - T$ equation of Müller et al. (2019). Data uncertainties are given as standard error (SE) for the $^{87}Sr/^{86}Sr$ ratios, $T\Delta_{47}$ and $\delta^{18}O_{water}$ respectively.

4.2. Fluid inclusions

Fluid inclusions in the dolomite crystals of the Huangliu Formation, mainly evident in the clear rims, are mostly <20 μm long and composed of water and gas (Supplementary Fig. 1). Given that most of the fluid inclusions cracked during the freezing and homogenization process, only one homogenization temperature of 37.2 °C from one fluid inclusion at 379.5 m bsl (Supplementary Fig. 1A) was obtained.

4.3. Stoichiometry

Dolostones in the Huangliu Formation are composed of low-Ca dolomite (LCD, <55%Ca) and high-Ca dolomite (HCD, >55%Ca) (Fig. 2B). Overall, the succession is formed mostly of HCD-dominated dolostones with an average %Ca = 55.4% (n = 103) (Fig. 2B). The percentage of LCD (%LCD) tends to be highest just below the unconformities (Fig. 2B). The %LCD increases with depth in unit 2, whereas in unit 3 the %LCD decreases with depth before increasing at a depth of ~350 m bsl (Fig. 2B). BSE images show that the inclusion-rich dark "dirty cores" of the dolomite crystals are typically composed of HCD with numerous micropores and calcite inclusions, whereas the clear rims are typically formed of LCD (Fig. 3C–H). The boundaries between the HCD core and LCD rim are sharp (Fig. 3C–H).

4.4. Oxygen isotopes

The $\delta^{18}O$ data for the dolostones of the Huangliu Formation reported in Wang et al. (2018) (determined in Guangxi University) were not corrected for the phosphoric acid fractionation factor of dolomite. After correcting the original $\delta^{18}O$ from Wang et al. (2018) using the fractionation factor of Rosenbaum and Sheppard (1986), the dolostones from the Huangliu Formation yielded $\delta^{18}O_{dol}$ values from 0.4 to 2.9‰ (average 1.8‰; n = 97) (Fig. 2E), which are ~1.5‰ lower than the original $\delta^{18}O$ values (2.0 to 4.7‰, average 3.3‰; n = 97) given in Wang et al. (2018). For the same dolostone samples in the Huangliu Formation, the corrected $\delta^{18}O_{dol}$ values tested in Guangxi University are consistent (positive correlation $R^2 = 0.86$) with those obtained by the China University of Geoscience (n = 22) (Supplementary Fig. 2A). The corrected $\delta^{18}O_{dol}$ values are used herein. The $\delta^{18}O_{dol}$ values of the dolomites of unit 1 (0.4 to 2.8‰; average 1.4‰) are slightly more negative than those from unit 2 (1.5 to 2.9‰; average 2.1‰), unit 3 (1.3 to 2.8‰; average 2.1‰), and unit 4 (1.3 to 2.3‰; average 1.8‰), respectively (Supplementary data).

4.5. Strontium isotopes

Integration of the $^{87}Sr/^{86}Sr$ data from Wang et al. (2018) with 27 new $^{87}Sr/^{86}Sr$ obtained in this study, shows that the $^{87}Sr/^{86}Sr$ ratios (n = 52), which range from 0.708898 to 0.709077, generally increase from the bottom to the top of the Huangliu Formation (Fig. 2C). As argued by Wang et al. (2018), this suggests that the dolomitization age becomes progressively younger toward the top of the formation (Fig. 8A). Overall, the $^{87}Sr/^{86}Sr$ ratios indicate that dolomitization took place ~10 to 4 Ma (late Miocene to early Pliocene) (>95% confidence interval): a narrower range than the ~10 to 2.3 Ma suggested by Wang et al. (2018). There are notable "jumps" in the $^{87}Sr/^{86}Sr$ values from 0.708929 to 0.708972 at depth of ~425 m bsl and from 0.708984 to 0.709038 at the depth of ~353 m bsl (Fig. 2C). According to the McArthur et al. (2001) LOWESS lookup curve, these two "jumps" of $^{87}Sr/^{86}Sr$ correspond to 7.4–8.1 Ma (~425 m bsl) and 5.3–5.8 Ma (~353 m bsl) respectively.

4.6. Clumped isotopes

After calibration to the ARF, the Δ_{47} values for the 22 dolostone samples with Mn/Sr <0.2 from the Huangliu Formation range from

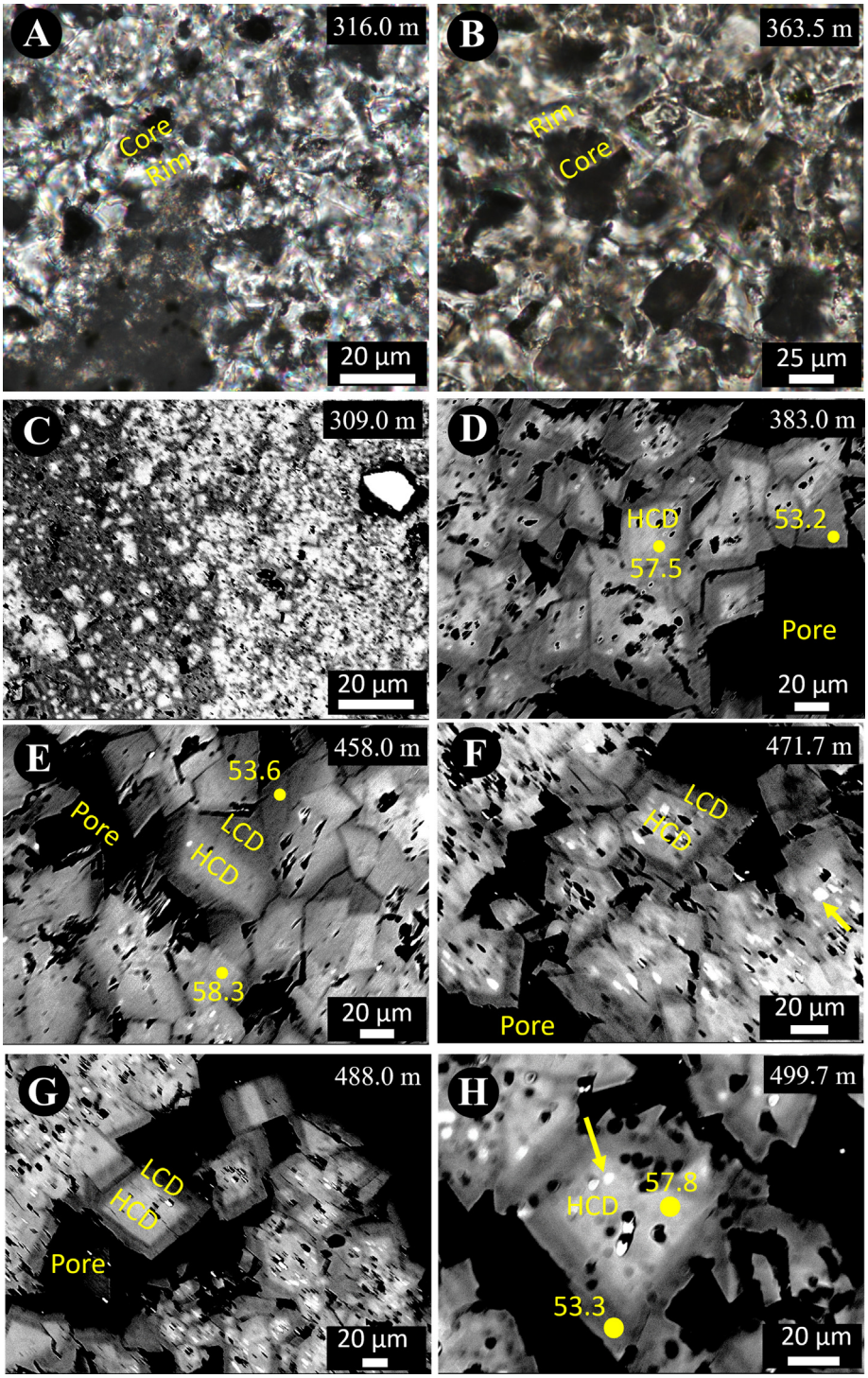

Fig. 3. Thin section photomicrographs (plane polarized light) (A–B) and backscatter images (C–H) of Huangliu dolostones from well CK-2, Xisha Islands. Depths specified in upper right corner of each image are below present-day sea-level. (A, B) Dolomite crystals with "dirty" cores encased by clean rims. (C) Contrast between dark low-Ca dolomite (LCD, <55%Ca) on the left side and bright high-Ca dolomite (HCD, >55%Ca) on the right side. (D–H) Different proportions of HCD and LCD in samples from different depths in well CK-2. Generally, the light gray HCD develops in the core of single dolomite crystal with dark irregular dissolved pores and bright residual calcite (yellow arrow), while the LCD grow on the outside of HCD and present dark gray color. Numbers in (D–H) represent the %Ca content of the spot analyzed by electron microprobe. (For interpretation of the references to color in this figure legend, the reader is referred to the web version of this article.)

0.67 to 0.73‰ at 90 °C acid digestion (Fig. 4A; Supplementary data). Using the Bonifacie et al. (2017) Δ_{47}-T calibration, which was based on the use of 90 °C acid digestion and similar analytical conditions to those used in this study, the calculated temperature derived from the clumped isotopes (T (Δ_{47})) ranges from 24 °C to 44 °C with an average of 31 ± 4 °C (Figs. 2F, 4B, 5C). Each T (Δ_{47}) is similar to, or 1–2 °C lower than, the temperature derived by Δ_{47} using the calibration of Müller et al. (2019), Petersen et al. (2019) or higher than Anderson et al. (2021) (Fig. 4B). The 1–2 °C difference between these calibrations is higher than the temperature errors (~2 °C) caused by analytical uncertainty (±0.010‰; 1 SE) of our samples. Combined with the oxygen isotope ($\delta^{18}O_{dol}$) and T (Δ_{47}) data (Bonifacie et al. calibration) from the Huangliu dolostones, the calculated $\delta^{18}O_{water}$ values derived using the equation of Müller et al. (2019) range from

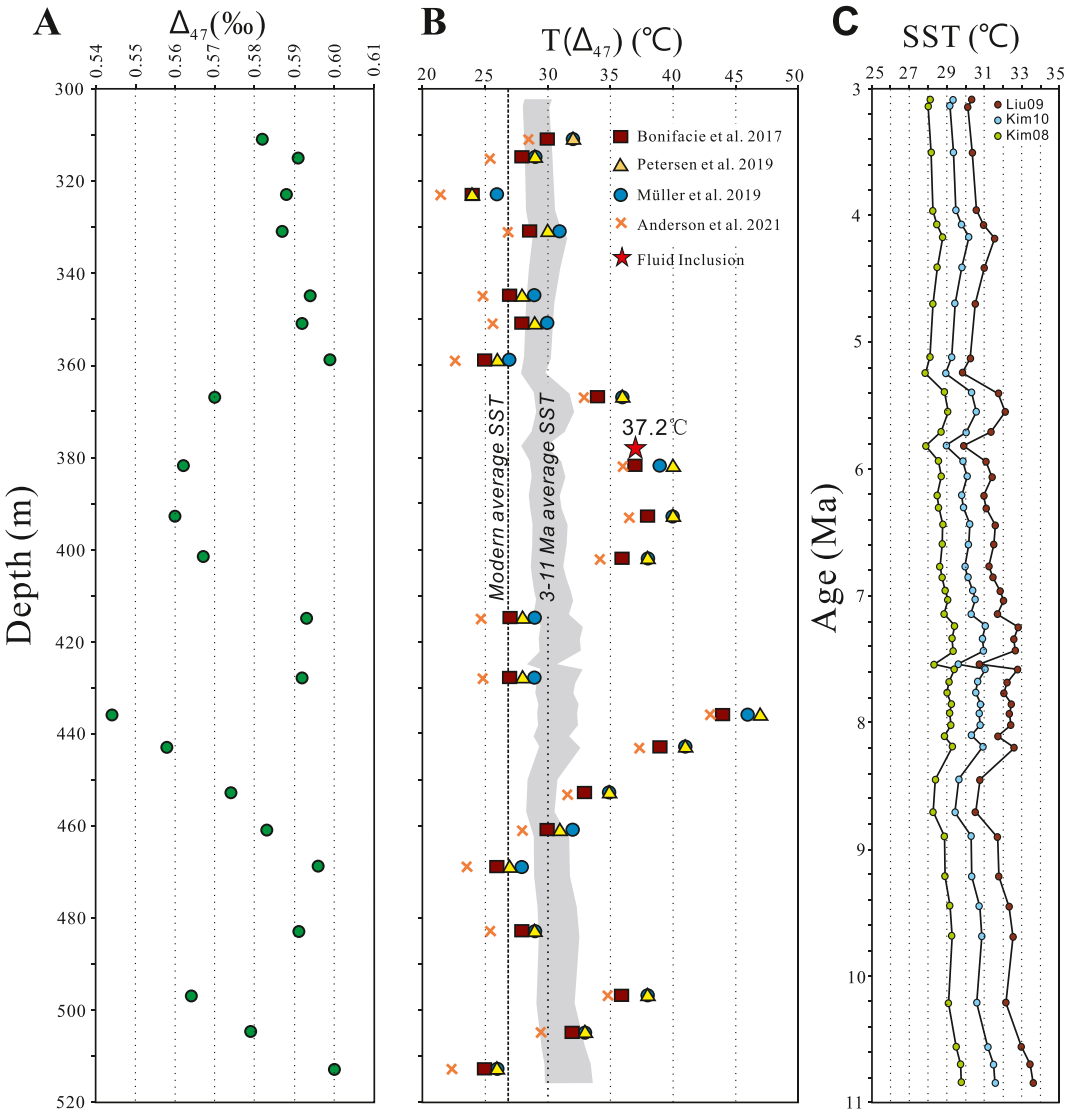

Fig. 4. (A) Clumped isotope (Δ_{47}) data for Huangliu dolostones. (B) Comparison of calculated temperature using the Δ_{47}-T calibrations from Bonifacie et al., 2017 for dolomite, Müller et al. (2019) for dolomite, and Petersen et al. (2019) for carbonate minerals, respectively. Red star represents the homogenization temperature of fluid inclusion at 379.5 m in the Huangliu dolostones. Gray shading represents the average surface seawater temperature (SST) showing in (C) during ~3 to 11 Ma in the South China Sea using the materials from ODP1143 (Zhang et al., 2014). (For interpretation of the references to color in this figure legend, the reader is referred to the web version of this article.)

1.1 to 4.5‰ (average 2.72‰; n = 22) (relative to the VSMOW scale) (Fig. 2G). The average 2.72‰ of $\delta^{18}O_{water}$ values derived from the equation of Müller et al. (2019) is generally lower than that of $\delta^{18}O_{water}$ values obtained using the Matthews and Katz (1977) equation (average 2.87‰; n = 22) and Vasconcelos et al. (2005) equation (average 2.94‰; n = 22) (Supplementary Fig. 3). The average 1.93‰ of $\delta^{18}O_{water}$ (n = 22) values derived using the equation of Horita (2014) is far lower than that from other three equations (Supplementary Fig. 3). There is a positive correlation (R^2 = 0.7) between the calculated T (Δ_{47}) and $\delta^{18}O_{water}$ for the dolostones of Huangliu Formation from well CK-2 (Fig. 6). Generally, the calculated T (Δ_{47}) and $\delta^{18}O_{water}$ values tend to be highest just below the unconformities and decrease away from the unconformities (Fig. 2F, G).

5. Discussion

5.1. Formation temperature of dolomites derived from clumped isotopes

Given that ordered dolomite has not been synthesized from normal seawater under low temperature (~25 °C) conditions (Land, 1998), the fractionation factor for the acid digestion reactions of dolomite between 25 and 90 °C (Δ^*_{90-25}) is still poorly constrained with Δ^*_{90-25} values ranging from 0.082 to 0.153‰ as determined from the same reference dolomite NIST 88b (Defliese et al., 2015; Murray et al., 2016; Bonifacie et al., 2017; Lu et al., 2022). Applying an acid fractionation correction for Δ_{47} analyses to dolomite can result in large uncertainties and produce erroneous temperature estimates (Müller et al., 2019). In order to avoid the Δ^*_{90-25} uncertainties associated with dolomite, the clumped isotope data at 90 °C acid digestion were standardized using the ARF as suggested by Dennis et al. (2011). Although many Δ_{47}-T calibrations had been proposed for carbonate minerals (e.g., Ghosh et al., 2006; Dennis and Schrag, 2010; Zaarur et al., 2013; Tang et al., 2014; Petersen et al., 2019; Anderson et al., 2021), only those proposed by Winkelstern et al. (2016), Bonifacie et al. (2017) and Müller et al. (2019) are dolomite specific. The calibration of Bonifacie et al. (2017) was used for discussion herein based on (1) it being derived using similar analytical conditions (e.g., 90 °C acid digestion temperature) to those used in this study, and (2) it has the minor calculated T(Δ_{47}) differences (~1–2 °C) with that obtained by using the calibrations of Müller et al. (2019), Petersen et al. (2019), and Anderson et al. (2021) (Fig. 4B).

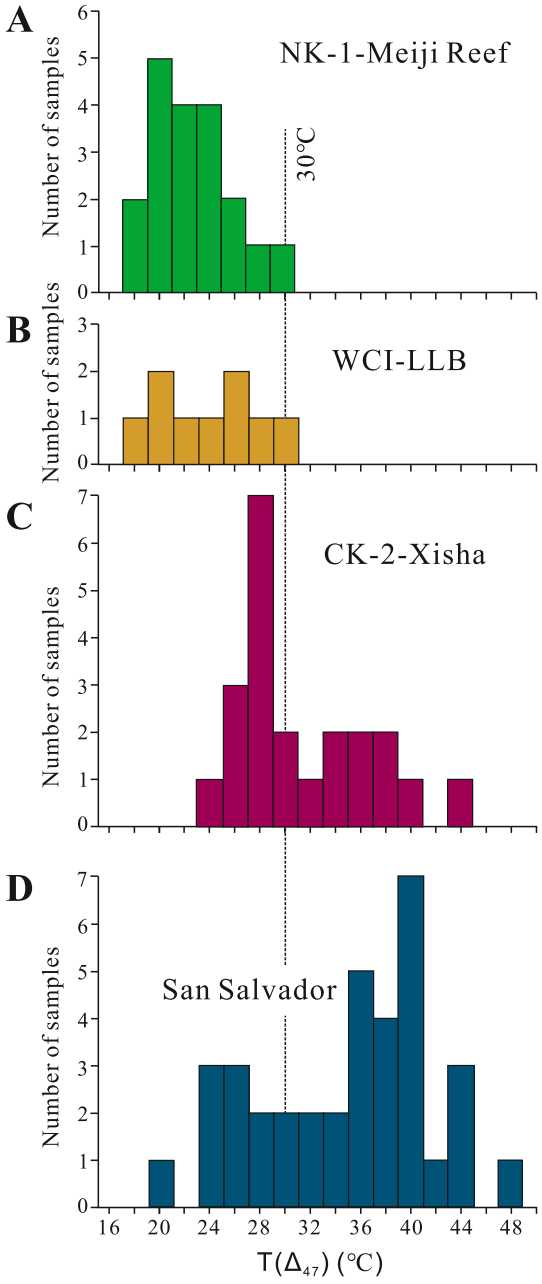

Fig. 5. Recalculated T(Δ_{47}) (°C) for dolostones from (A) well NK-1, Meiji Reef, (B) well WCI, Little Bahama Bank, (C) well CK-2, Xisha Islands, and (D) San Salvador using the Bonifacie et al. (2017) Δ_{47}-T calibration. The clumped isotopes (Δ_{47}) data were calibrated to an absolute reference frame (AFR) (Dennis et al., 2011) to avoid the instrument error between different laboratories. Original Δ_{47} data of dolostones are from Guo et al. (2021) (NK-1, Meiji Reef) and Murray and Swart (2017) (WCI, Little Bahama Bank and San Salvador).

Using the Δ_{47}-T calibration of Bonifacie et al. (2017), the average formation T(Δ_{47}) of 31 ± 4 °C for the dolostones in the Huangliu Formation is ~5 °C higher than the modern annual mean sea surface temperature (SST) of 26.8 °C around the Xisha Islands (Fig. 4B). When the dolostones of the Huangliu Formation formed during the late Miocene to early Pliocene, at ~10 to 4 Ma, the global air temperature may have been 3–7 °C higher than today (Collins et al., 2013; Fedorov et al., 2013). Similarly, at the ODP 1143 site (Fig. 1A), located in the south part of the South China Sea ~815 km from well CK-2, analysis of the deep-sea sediments indicates that the mean SST was ~31 °C between ~11 and 3 Ma, which is ~4 °C higher than the average modern SST in that area (Zhang et al., 2014) (Fig. 4B, C). Thus, the calculated average T(Δ_{47}) of the Huangliu dolostones is consistent with the SST that existed during the late Miocene to early Pliocene. In addition, the homogenization temperature of 37.2 °C, derived from one fluid inclusion at 379.5 m bsl (Supplementary Fig. 1A), is similar to the calculated T(Δ_{47}) of 38.9 °C at 382 m bsl obtained from the Huangliu Formation.

The reliability of the calculated T(Δ_{47}) depends on the Δ_{47} value of the Huangliu dolostones and assumes that there was minimal solid-state reordering of ^{13}C–^{18}O during diagenesis (Dennis and Schrag, 2010; Henkes et al., 2014; Stolper and Eiler, 2015; Hemingway and Henkes, 2021). Potentially, the solid-state reordering of ^{13}C–^{18}O, which could influence the amount of ^{13}C–^{18}O in the carbonate mineral crystal lattices, could occur if the ambient temperature around the carbonate rocks was >100 °C over a period of tens of millions of years (Dennis and Schrag, 2010; Passey and Henkes, 2012; Henkes et al., 2014). Geothermal gradients reported from isolated Cenozoic islands range from ~−20 °C·km^{-1} for Enewetak Atoll in the equatorial Pacific Ocean (Saller, 1984), ~10 °C·km^{-1} for the Nansha Islands in the South China Sea (Wang et al., 2020), to ~15 °C·km^{-1} for the Bahamian platform (Epstein and Clark, 2009). Based on these figures, especially the geothermal gradients of Nansha Islands in the South China Sea (Wang et al., 2020), the deepest part of the Huangliu Formation in CK-2 (~520 m) probably experienced a maximum burial temperature of no more than 50 °C. There are no reports that the modern deep stratum temperatures associated with carbonate rocks (wells Xike-1 and Xichen-1) (<1 km) in Xisha Islands are higher than 50 °C (Zhao, 2010; Shao et al., 2017a, 2017b; Bi et al., 2018). The influence of solid-state reordering on clumped isotopes has not been deemed important for other Cenozoic island dolostones that have not been buried >1 km (Winkelstern and Lohmann, 2016; Murray and Swart, 2017; Guo et al., 2021).

Island dolostones, like those in the Huangliu Formation, formed largely through replacement of precursor limestones (Budd, 1997; Ren and Jones, 2018). There is also the possibility, however, that some of the dolostones may have been subsequently modified by diagenesis (Budd, 1997). If diagenetic alteration (recrystallization and/or cementation) occurred, the temperature signal derived from the Δ_{47} value of island dolostones may reflect, at least in part, diagenetic recrystallization and/or cementation (Huntington et al., 2011). Although most sedimentary dolostones are susceptible to recrystallization, the dolostones in the Huangliu Formation do not display obvious evidence of recrystallization given that they are characterized by (1) fabric retentive textures in units 2 to 4, (2) nonstoichiometric (Ca-rich) compositions (Fig. 2B), (3) dolomite crystals that are commonly zoned with cores of HCD encased by rims of LCD (1–10 μm thick) with sharp boundaries between successive zones (Fig. 3D–H), and (4) low Mn/Sr ratios (0.1 to 0.9) (Fig. 2D) (Wang et al., 2018, 2021). Veillard et al. (2019) suggested that the shallow burial recrystallization was responsible for the increase in the T(Δ_{47}) with depth in the Marion Plateau dolostones (NE Australia). For the Huangliu dolostones, however, there is no increase in the T(Δ_{47}) with depth overall or in each unit (e.g., unit 2) (Fig. 2F).

It is possible that the diagenetic cementation that occurred in dolostones of the Huangliu Formation may have influenced the temperature signal derived from the Δ_{47} values. The LCD components, that presented as the inclusion-free outer rims around many of the dolomite crystals (Fig. 3), are evidence for widespread modification of the dolostones in the Huangliu Formation (Fig. 2B). Such rims have generally been treated as cements that precipitated from the pore fluids (Budd, 1997; Jones, 2005, 2007), and probably formed after the primary replacement of the limestone precursor. Choquette and Hiatt (2008) argued that the dolomitization of the original limestone followed by dolomite cementation ('overdolomitization') may produce dolomite crystals that have a cloudy core encased by a clear rim. In addition, the T(Δ_{47}) of the samples with LCD >80% (n = 6) in the Huangliu Formation yielded an average T of ~34 °C, whereas those dolostones formed entirely of HCD (HCD = 100%; n = 7) produced an average T of ~27 °C (Fig. 7). Consequently, the HCD cores in the Huangliu Formation may be

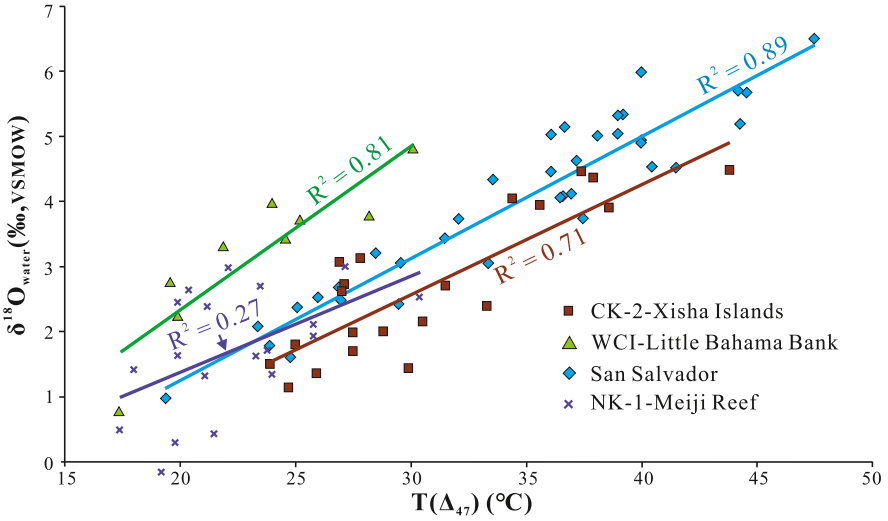

Fig. 6. Relationship between $\delta^{18}O_{water}$ (‰, VSWOM) and T(Δ_{47}) (°C) for the dolostones from wells NK-1 (Meiji Reef), WCI (Little Bahama Bank), CK-2 (Xisha Islands), and San Salvador. High positive correlation between $\delta^{18}O_{water}$ and T(Δ_{47}) exists in the dolostones from CK-2, WCI, and San Salvador, but not for NK-1. The $\delta^{18}O_{water}$ and T (°C) data from NK-1 (Guo et al., 2021), WCI and San Salvador (Murray and Swart, 2017) were all recalculated using the Müller et al. (2019) $10^3 \ln\alpha - T$ equation and Bonifacie et al. (2017) Δ_{47}-T calibration. See Supplementary data for details.

representative of the primary replacive dolomite whereas the LCD cements formed later and possibly under different conditions. The low correlation ($R^2 = 0.27$) between T(Δ_{47}) and the average %Ca of the dolomites (Supplementary Fig. 2B), suggests that the T(Δ_{47}) difference between the HCD cores and LCD cements is not related to %Ca content. Collectively, this indicates that dolomitization of the original limestones may have been achieved under lower temperatures than those associated with the later precipitation of the dolomite cements.

Using the Δ_{47}-T calibration of Bonifacie et al. (2017), the recalculated values derived from the clumped isotopes of the dolostones from NK-1 of Meiji Reef in the South China Sea (Guo et al., 2021), WCI–Little Bahamas Bank, and San Salvador (Murray and Swart, 2017) (Fig. 5; Supplementary data) show that the T(Δ_{47}) values derived from the dolostones from the Xisha Islands (24 to 44 °C, average 31 °C) and San Salvador (19 to 48 °C, average 36 °C) are higher than those from the NK-1-Meiji Reef (17 to 30 °C, average 22 °C) and WCI-Little Bahamas Bank (17 to 30 °C, average 23 °C) (Fig. 5). Although the factors that controlled the different T(Δ_{47}) of dolostones from these islands are complex and difficult to define, they probably include paleo-location, local paleoclimate, burial depths, and local thermal convection history that existed when dolomitization took place. Although these factors are impossible to quantify with currently available data, it does appear that temperature was not a critical factor in the island near-surface dolomitization process.

5.2. Salinity of dolomitization fluids based on T(Δ_{47})

The salinity of the water that mediated dolomitization can be inferred from the $\delta^{18}O_{water}$ given that this value becomes more positive with increased evaporation (Belem et al., 2019). Many different equations have been used to calculate the $\delta^{18}O_{water}$ by using the $\delta^{18}O_{dol}$ and temperature data (Northrop and Clayton, 1966; O'Neil and Epstein, 1966; Fritz and Smith, 1970; Sheppard and Schwarcz, 1970; Matthews and Katz, 1977; Zheng, 1999; Vasconcelos et al., 2005; Horita, 2014; Müller et al., 2019). Here, the equations proposed by Müller et al. (2019), Vasconcelos et al. (2005), Horita (2014), and Matthews and Katz (1977) are used to calculate the $\delta^{18}O_{water}$ for the dolostones from the Huangliu Formation in well CK-2 because (1) the first two equations contain low temperature (25 and 45 °C) formation regimes of natural dolomite as opposed to high temperature experiments (>80 °C), and (2) the equation from Matthews and Katz (1977) and Horita (2014) was used in the study of the Bahamian dolostones (Winkelstern and Lohmann, 2016; Murray et al., 2016). Given that the calculated $\delta^{18}O_{water}$ values from the equation of Horita (2014) are lower than the values derived from the other three equations that yielded minimal differences (~0.1 to 0.3‰) (Supplementary Fig. 3), the latest equation proposed by Müller et al. (2019) was used to calculate the $\delta^{18}O_{water}$ (1.1 to 4.5‰ with average 2.72‰ VSMOW) for the dolostones from the Huangliu Formation in well CK-2.

Compared to the $\delta^{18}O_{water}$ (0 ± 2‰; VSMOW) of Cenozoic seawater at near-Earth-surface temperatures (<30 °C) (Zachos et al., 2001) and/or the Miocene seawater value of $\delta^{18}O_{water}$ (−1.2‰) (Kennett and Shackleton, 1975), the $\delta^{18}O_{water}$ values (1.1 to 4.5‰ – average 2.72‰; VSMOW) derived from the Huangliu dolostones imply that normal to slightly evaporated seawater ($\delta^{18}O_{water}$ > 2‰) mediated dolomitization. Many studies, including those by Budd (1997) and Ren and Jones (2018), have relied at least in part, on interpretation of $\delta^{18}O$ values of island dolostones to suggest that normal to slightly evaporated seawater mediated dolomitization. The distinction between normal seawater and slightly evaporated seawater based on $\delta^{18}O$ alone, however, is difficult because of uncertainties associated with interpretations of $\delta^{18}O$ values (Budd, 1997; Ren and Jones, 2018).

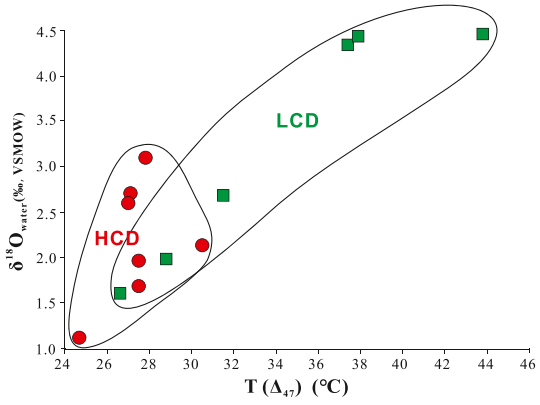

Fig. 7. Cross-plots of $\delta^{18}O_{water}$ (‰, VSWOM) and T(Δ_{47}) (°C) for samples with LCD > 80% (n = 6) and pure HCD (HCD = 100%; n = 7) from the Huangliu Formation in well CK-2, Xisha Islands.

Given that the dolomite crystals in the Huangliu Formation are commonly zoned, the calculated $\delta^{18}O_{water}$ is an average value that reflects the primary replacive HCD and the LCD cements that formed later. Application of the Müller et al. (2019) equation to the samples with LCD >80% (n = 6) indicates formation from water that had an average $\delta^{18}O_{water}$ of 3.2‰. Fluid inclusions found in the clear rims of the dolomite crystals in the same formation from well XK-1 on Xisha Islands (~81 km NE of well CK-2) indicate that seawater with a higher salinity seawater mediated dolomitization (Bi et al., 2018). In contrast, for samples formed entirely of HCD (n = 7) in well CK-2, the formative water had a lower average $\delta^{18}O_{water}$ of 2.2‰ (Fig. 7). This implies that the primary replacement dolomites may have been formed in lower salinity fluids than those related to dolomite cements that formed later.

Based on the recalculated T(Δ_{47}) values for the dolostones from the NK1-Meiji Reef, WCI-Little Bahamas Bank, and San Salvador and use of the Müller et al. (2019) equation, the newly recalculated $\delta^{18}O_{water}$ values are −0.2 to 3.0‰ (average 1.72‰; n = 19), 0.8 to 4.8‰ (average 3.2‰; n = 9), and 1.0 to 6.5‰ (average 4.0‰; n = 36), respectively (Fig. 6; Supplementary data). Given that the main source of the Mg needed for dolomitization (e.g., Budd, 1997), the calculated $\delta^{18}O_{water}$ values of these dolostones represent normal to slightly evaporated seawater, suggesting that no obvious other fluid types were involved in the fluids that mediated dolomitization on these islands. It also seems that this applies irrespective of the temperatures that were involved (Fig. 6).

5.3. Cement formation

Available evidence indicates that the clear LCD rims that encase the "dirty" cores of the dolomite crystals probably formed at a later time and possibly under different diagenetic conditions. As suggested by Choquette and Hiatt (2008), cementation events in pre-Holocene dolomites, can follow 'replacement dolomitization' events by time intervals ranging from geologically 'instantaneous' to tens of million years. This means that formation of the dolomite cements should be considered separately from the formation of the dirty cores. For the Huangliu dolostones, the HCD cores seem to be genetically linked to seawater (average 2.2‰ of $\delta^{18}O_{water}$) in near-surface environments (average ~27 °C). In contrast, the LCD cements probably formed from slightly evaporated seawater (average 3.2‰ of $\delta^{18}O_{water}$) under slightly higher temperature (average ~34 °C) conditions. This tacitly implies that a two-stage dolomitization process led to the formation of the Huangliu dolostones and other similar island dolostones.

Based on comparisons with Cenozoic seawater (<30 °C, $\delta^{18}O_{water}$ = 0 ± 2‰ – Zachos et al., 2001), the LCD cements may have formed under shallow burial conditions or in an area where there was active evaporation of the diagenetic fluids.

- The fact that the T(Δ_{47}) of the dolostones in the Huangliu Formation does not increase with burial depth or systematically from unit to unit (Fig. 2E), indicates that dolomitization was mediated by fluids with relatively constant temperatures.
- On isolated carbonate platforms, like the Xisha Islands, evaporative seawater is typically attributed to development in a lagoon under a semi-arid to arid climate (Budd, 1997). During the late Miocene to early Pliocene, the global air temperature was 3–7 °C higher than today (Collins et al., 2013; Fedorov et al., 2013) and the progressively drier climate (e.g., Zachos et al., 2001; Casanovas-Vilar, 2014; Roveri et al., 2014; Herbert et al., 2016) may have led to evaporation of seawater. Although only a few isolated carbonate buildups existed on the Xisha platform (Wu et al., 2014), there is evidence that lagoonal environments developed on top of Xuande Atoll (Zhang et al., 1989). The absence of evaporite minerals (e.g., gypsum, halite) in the Huangliu Formation and the overlying Yinggehai Formation and Ledong Formation, however, indicates that (1) the lagoon was not completely closed off from the open ocean and hypersaline seawater was never generated, or (2) the evaporate minerals were removed by erosion and/or meteoric dissolution during the following decline of sea-level.
- The fact that the LCD cements are most common beneath the unconformities/exposure surfaces (Fig. 2B) may indicate that they were related to the decline of relative sea-level.

It is possible that slightly evaporated seawater, which formed in a lagoon, may have been responsible for the formation of the LCD cements. Simms (1984) and Kaufman (1994) argued that even slight increases in salinity (38–42‰) are sufficient to generate large-scale reflux of waters through carbonate platforms and below carbonate islands. Overall, the notion that the abundance of LCD cements, and the values of $\delta^{18}O_{water}$ and T (Δ_{47}) decrease with depth below the unconformities/exposure surfaces (e.g., in units 1–3) (Fig. 2) seems to be consistent with dolomitization being due to the reflux of slightly evaporative seawater. Many studies have suggested that the large-scale dolomitization of ancient limestones in shallow sea settings, which lack obvious evidence of evaporites, may be related to the reflux infiltration of seawater with elevated salinity (Sun, 1994; Qing, 1998; Qing et al., 2001; Melim and Scholle, 2002; Eren et al., 2007; Rameil, 2008).

The positive correlation ($R^2 = 0.7$) between T(Δ_{47}) and $\delta^{18}O_{water}$ for dolostones in the Huangliu Formation from well CK-2 (Fig. 6) is similar to that reported from many Cenozoic island dolostones including those from the Little Bahama Bank and San Salvador (Murray et al., 2016), the Marion Plateau (Veillard et al., 2019) (Fig. 6), and some ancient carbonate minerals/components (Cummins et al., 2014; Henkes et al., 2018). Cummins et al. (2014) suggested that the positive relationship between $\delta^{18}O_{water}$ and T(Δ_{47}) may indicate that recrystallization of the carbonate minerals/components occurred in rock-buffered diagenetic environments. Veillard et al. (2019) also argued that the positive correlation between $\delta^{18}O_{water}$ and T(Δ_{47}) in the Marion Plateau dolostones was evidence of shallow burial recrystallization via dissolution/reprecipitation in a closed diagenetic system. Although there is evidence for the widespread development of dolomite cements in the dolostones of the Huangliu Formation, there is no clear petrography evidence that any recrystallization took place. Thus, the positive relationship between T(Δ_{47}) and $\delta^{18}O_{water}$ in the dolostones in the Huangliu Formation in well CK-2 may imply that both the LCD and HCD formed in a low water–rock ratio diagenetic system. Theoretically, in such an environment, the $\delta^{18}O_{carbonate}$ values will remain stable even though the water temperature and $\delta^{18}O_{water}$ may both vary (e.g., Cummins et al., 2014; Veillard et al., 2019). For the LCD cements, based on the equation $Ca^{2+} + Mg^{2+} + CO_3^{2-} = CaMg(CO_3)_2$ for cement formation (Warren, 2000), it would seem that the CO_3^{2-} for the formation of LCD probably came from the precursor limestones. If the CO_3^{2-} came mainly from the evaporative seawater, there would not be a positive correlation between T(Δ_{47}) and $\delta^{18}O_{water}$.

5.4. Dolomitization and sea-level change

Many Cenozoic island dolostones in the Pacific Ocean and the Caribbean Sea that formed under near-Earth-surface conditions have been commonly linked to global sea-level changes (e.g., Budd, 1997; Ren and Jones, 2018). Sea-level fluctuations during the late Miocene to early Pliocene, for example, may have been greater than 50 m (Miller et al., 2005) or 100 m (Haq et al., 1987). Given that the Huangliu dolostones formed under near-sea-surface conditions (e.g., 24 to 44 °C and normal to slightly evaporated seawater) and probably in close proximity to unconformities/exposure surfaces (Fig. 2A), it seems that dolomitization may have been influenced by sea-level changes. Based on $^{87}Sr/^{86}Sr$ ratios from the dolostones in the Huangliu Formation, Wang et al. (2018) suggested that a (semi-) continuous "time-transgressive" dolomitization process, related to the combined effects of tectonic subsidence and/or eustatic sea-level changes, was responsible for the pervasive dolomitization of the succession. Integration of the $^{87}Sr/^{86}Sr$

from Wang et al. (2018) with the 27 new $^{87}Sr/^{86}Sr$ obtained in this study suggests that the dolomitization of the precursor limestones started ~10 Ma and continued until ~4 Ma, but with pauses between 7.4–8.1 Ma and 5.3–5.8 Ma (Fig. 8A). Since the Xisha Platform was initiated during the early Miocene (~20 Ma), the surrounding basins experienced constant tectonic subsidence from the late Miocene to early Pliocene (Wu et al., 2014). During the periods 7.4–8.1 Ma and 5.3–5.8 Ma, the rate of tectonic subsidence seems to have been relatively constant (Wu et al., 2014; their Fig. 10), which implies that subsidence was not the main factor that caused the pause in the dolomitization of limestones in the Huangliu Formation.

Various global eustatic sea-level curves (Vail and Mitchum, 1979; Haq et al., 1987; Miller et al., 2005) (Fig. 8D, E) and local relative sea-level curves (Wei et al., 2001; Thompson and Abbott, 2003; Pang et al., 2005) (Fig. 8B, C) for the South China Sea had been proposed for the late Cenozoic. The timing and amplitude of these curves, which vary in the scope and timing of sea-level fluctuations, are difficult to link directly to dolomitization ages. Nevertheless, the discontinuation of dolomitization between 5.3 Ma and 5.8 Ma is consistent with the Messinian Salinity Crisis (MSC) (5.33 to 5.96 Ma). The notion of episodic dolomitization during the MSC period has also been suggested for the successions found on Kati-daito-jima and the Great Barrier Reef (Ohde and Elderfield, 1992; McKenzie et al., 1993; Wang et al., 2019). Although no clear record of the impact of the MSC on Late Miocene climate has been identified (Roveri et al., 2014), the sea-level on many Cenozoic islands during the MSC was considerably lower than it is today (e.g., 30 to 100 m lower) (Ohde and Elderfield, 1992; Pigram et al., 1992; Aharon et al., 1993; Jones and Hunter, 1994; Wheeler and Aharon, 1997). In most of those curves (e.g., Vail and Mitchum, 1979; Haq et al., 1987; Wei et al., 2001; Pang et al., 2005), the onset of dolomitization at ~10 Ma followed a lowstand period (~9.5 to 10 Ma) and the pause in dolomitization at 7.4–8.1 Ma may correspond to a lowstand period. Some care must be taken with these interpretations because (1) the true sea-level position during the MSC is still not known with certainty with ranges from −30 to 100 m being proposed, and (2) on many oceanic islands, there is no direct evidence of the sea-level position during times when dolomitization was taking place and such sea-level positions must then be inferred from evidence from elsewhere in the world. The situation is further compounded in the case of the Xisha Islands where rapid subsidence has been the norm since the Early Miocene.

Apart from the discontinuities in the dolomitization ages, the semi-continuous "time-transgressive" dolomitization process evident from the Huangliu Formation (Wang et al., 2018) was probably linked to eustatic transgressive conditions in the Xisha area. With the data that are currently available, it is difficult to determine if tectonic subsidence and/or eustatic sea-level were responsible for that transgressive phase. Nevertheless, the presence of replacive HCD and LCD cements that formed under different temperature and salinity regimes, suggests that eustatic sea-level changes may have played a crucial role for their formation.

5.5. Implication for dolomitization models

Critical elements of all dolomitization models are a supply of Mg, a mechanism for circulating that Mg through the limestones, and sites that are conducive to the formation of dolostone (Morrow, 1982a, 1982b). In the case of island dolostones, many different models such as tidal pumping, seepage influx, and brine reflux, have been proposed (Budd, 1997). None of these models, however, can explain the difference of formation temperature, salinity, and the dual aspects of the replacive HCD and the LCD cements in the dolostones of the Huangliu Formation. Whitaker et al. (2004), however, emphasized that it may be misleading to conceptualize individual flow mechanisms for dolomitization in isolation, because fluid flow regimes in various geologic settings may be a function of a number of different drivers that act simultaneously or consecutively. Available evidence indicates that two processes were involved in the formation of the Huangliu dolostones – one that created the HCD cores of the crystals (Stage-I) and other that produced the clear LCD rims (Stage-II) (Fig. 9). During the dolomitization phase, that may have lasted for several million years (e.g., 4 to 10 Ma), the associated sea-level changes may have led to the different

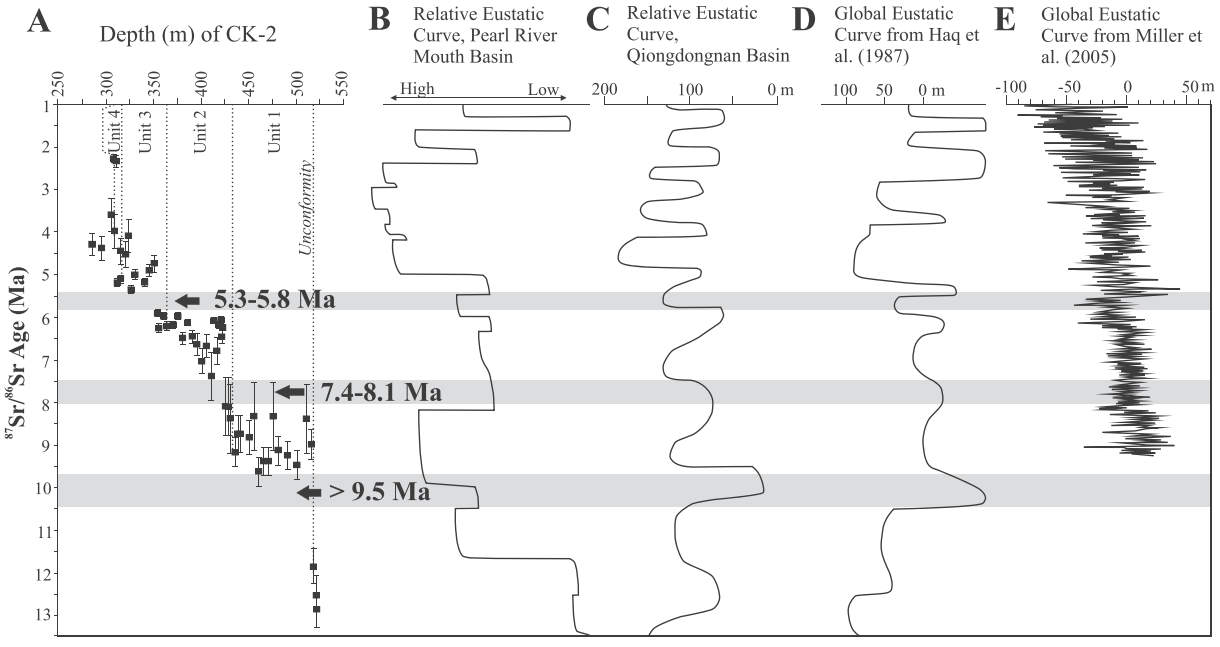

Fig. 8. Relationship between age of dolomitization in the Huangliu Formation and relative global and local sea-level curves. (A) Dolomitization ages of Huangliu Formation determined by $^{87}Sr/^{86}Sr$ ratios using McArthur et al. (2001) LOWESS lookup data. (B) Relative eustatic curve for Pearl River Basin, north South China Sea, from Pang et al. (2005, their Fig. 5). (C) Relative eustatic curve of Qiongdongnan Basin, north South China Sea from Wei et al. (2001, their Fig. 2). (D) and (E) Global eustatic curves from Haq et al. (1987, their Fig. 2) and Miller et al. (2005, their Fig. 4), respectively.

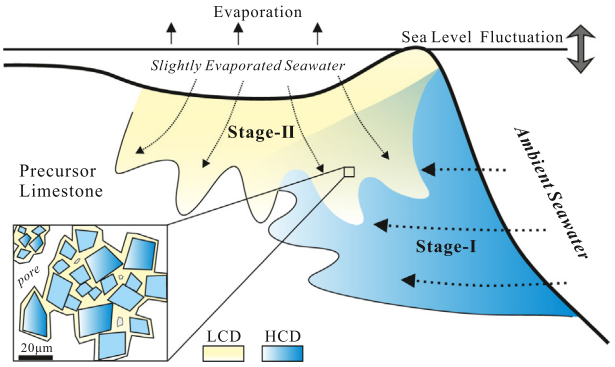

Fig. 9. Two dolomitization processes for the Miocene Huangliu dolostones in the Xisha Islands, South China Sea. Concentric ambient seawater flow through the platform (adopted from the concept of dolomitization models from Ren and Jones, 2018) for the formation of HCD (Stage-I). Slightly evaporative seawater flow downward for the formation of LCD (Stage-II). The two-stage dolomitization processes could be reciprocating action due to sea-level fluctuations.

salinity, temperature, and hydrology of the water that flowed through the Xisha platform. The "normal" seawater (Stage-I) and "evaporative" seawater (Stage-II) stages, with different flow mechanisms may have acted successively on the precursor limestone to produce replacive dolomites and dolomite cements respectively. Hence, the repetitive vertical stacked styles of T(Δ_{47}), $\delta^{18}O_{water}$ and LCD% (HCD%) in the dolostones of Huangliu Formation (Fig. 2) may reflect the reciprocating action of the two-stage dolomitization processes associated with sea-level fluctuations.

Given that Cenozoic island dolostones in the Pacific Ocean, Caribbean Sea, and South China Sea have been considered globally synchronized (e.g., Budd, 1997; Ren and Jones, 2018; Wang et al., 2019), this two-stage dolomitization process may be a phenomenon that was common to all Cenozoic island dolostones. For example, Murray and Swart (2017) also argued that the dolostones on Bahamian platform probably formed by different mechanisms driving normal marine seawater and evaporative brine through the rocks. The primary replacive dolomites and dolomite cements are also widespread in the dolostones from Cayman Islands (e.g., Jones, 2005, 2007; Zhao and Jones, 2012), thus the two-stage dolomitization process probably also existed on them.

The temperature and salinity of the fluids derived from clumped isotopes indicate that the Huangliu dolostones formed under near-sea-surface conditions. Since this study only involves the data from one core, it is difficult to determine the geographical variation of the temperature and salinity of replacive dolomites and dolomite cements on a platform scale, and hence determine the hydrological systems responsible. The two-stage dolomitization processes proposed for the Huangliu dolostones, however, clearly indicate that pervasive dolomitization on these islands needs composite flow systems that drive large volumes of seawater through the platform. For a comprehensive understanding of these processes, further clumped isotope data of island dolostones are required – both from the same island and from different islands.

6. Conclusions

Clumped isotopes and oxygen isotopes indicate that the Huangliu dolostones in the Xisha Islands, South China Sea formed from normal to slightly evaporated seawater with water temperatures between 24 and 44 °C. This conclusion should be treated with some caution because the clumped isotope thermometry of the dolostones may have been influenced by the precipitation of the outer LCD cortex that probably formed some time after the replacive dolomite had formed. Available data indicates that late dolomite cements may have formed from seawater that was warmer and may have experienced more evaporation than the near-surface seawater that may have mediated the earlier formed primary replacive dolomites. Those two contrasting types of dolomites in the same crystal are difficult to interpret by any single dolomitization model. Accordingly, a two-stage dolomitization model, related to sea-level changes that promoted temperature and salinity changes in the seawater that mediated the dolomitization is invoked. A similar model may also have been responsible for the development of other Cenozoic island dolostones.

Supplementary data to this article can be found online at https://doi.org/10.1016/j.sedgeo.2021.106079.

Declaration of competing interest

The authors declare that they have no known competing financial interests or personal relationships that could have appeared to influence the work reported in this paper.

Acknowledgement

This work was funded by the National Natural Science Foundation of China (Nos. 41962010, 42030502, and 42090041), Guangxi Science and Technology Planning Project (Nos. AD17129063 and AA17204074), and Open Fund Project of Key Laboratory of Carbonate Reservoirs, CNPC (RIPED-2021-JS-1731). We thank Jun Li and Shanghua Si from Xi'an Petroleum University for helping to test the fluid inclusions, and Junhua Huang from State Key Laboratory of Biogeology and Environmental Geology, China University of Geosciences for the analysis of clumped isotopes. We are also grateful to Wei Jiang, Shendong Xu, and Tianlai Fan from Guangxi University for acquiring the data of elements, oxygen isotopes and Sr isotopic ratios respectively. We also thank to an anonymous reviewer, Dr. Winkelstern and Editor Dr. Knight for their valuable suggestions improving this paper.

References

Aharon, P., Goldstein, S.L., Wheeler, C.W., Jacobson, G., 1993. Sea-level events in the South Pacific linked with the Messinian salinity crisis. Geology 21, 771–775.

Anderson, N.T., Kelson, J.R., Kele, S., Daëron, M., Bonifacie, M., Horita, J., Mackey, T.J., John, C.M., Kluge, T., Petschnig, P., Jost, A.B., Huntington, K.W., Bernasconi, S.M., Bergmann, K.D., 2021. A unified clumped isotope thermometer calibration (0.5-1,100 °C) using carbonate-based standardization. Geophysical Research Letters 48, e2020GL092069. https://doi.org/10.1029/2020GL092069.

Belem, A.L., Caricchio, C., Albuquerque, A.L.S., Venancio, I.M., Zucchi, M.D.R., Santos, T.H.R., Alvarez, Y.G., 2019. Salinity and stable oxygen isotope relationship in the Southwestern Atlantic: constraints to paleoclimate reconstructions. Anais da Academia Brasileira de Ciências 91, e20180226. https://doi.org/10.1590/0001-3765201920180226.

Bi, D., Zhai, S., Zhang, D., Liu, X., Liu, X., Jiang, L., Zhang, A., 2018. Constraints of fluid inclusions and C, O isotopic compositions on the origin of the dolomites in the Xisha Islands, South China Sea. Chemical Geology 493, 504–517.

Bonifacie, M., Calmels, D., Eiler, J.M., Horita, J., Chaduteau, C., Vasconcelos, C., Agrinier, P., Katz, A., Passey, B.H., Ferry, J.M., Bourrand, J.J., 2017. Calibration of the dolomite clumped isotope thermometer from 25 to 350 °C and implications for a universal calibration for all (Ca, Mg, Fe) CO_3 carbonates. Geochimica et Cosmochimica Acta 200, 255–279.

Budd, D.A., 1997. Cenozoic dolomites of carbonate islands: their attributes and origin. Earth-Science Reviews 42, 1–47.

Casanovas-Vilar, I., 2014. The range and extent of the Vallesian Crisis (Late Miocene): new prospects based on the micromammal record from the Vallès-Penedès basin (Catalonia, Spain). Journal of Iberian Geology 40, 29–48.

Chang, B., Li, C., Liu, D., Foster, I., Tripati, A., Lloyd, M.K., Maradiaga, I., Luo, G.M., An, Z.H., She, Z.B., Xie, S.C., Tong, J.N., Huang, J.H., Algeo, T.J., Lyons, T.W., Immenhauser, A., 2020. Massive formation of early diagenetic dolomite in the ediacaran ocean: constraints on the "dolomite problem". Proceedings of the National Academy of Sciences 117, 14005–14014.

Choquette, P.W., Hiatt, E.E., 2008. Shallow-burial dolomite cement: a major component of many ancient sucrosic dolomites. Sedimentology 55, 423–460.

Collins, M., Knutti, R., Arblaster, J., Dufresne, J.L., Fichefet, T., Friedlingstein, P., Gao, X., Gutowski, W.J., Johns, T., Krinner, G., Shongwe, M., Tebaldi, C., Weaver, A.J., Wehner, M., 2013. Long-term climate change: projections, commitments and irreversibility. In: Stocker, T.F., Qin, D., Plattner, G.K., Tignor, M., Allen, S.K., Boschung, J., Nauels, A., Xia, Y., Bex, V., Midgley, P.M. (Eds.), The Physical Science Basis. Contribution of Working Group I to the Fifth Assessment Report of the Intergovernmental Panel on Climate Change. Cambridge University Press, Cambridge, United Kingdom, pp. 1029–1136.

Cummins, R.C., Finnegan, S., Fike, D.A., Eiler, J.M., Fischer, W.W., 2014. Carbonate clumped isotope constraints on Silurian ocean temperature and seawater $\delta^{18}O$. Geochimica et Cosmochimica Acta 140, 241–258.

Defliese, W.F., Hren, M.T., Lohmann, K.C., 2015. Compositional and temperature effects of phosphoric acid fractionation on Δ_{47} analysis and implications for discrepant calibrations. Chemical Geology 396, 51–60.
Dennis, K.J., Schrag, D.P., 2010. Clumped isotope thermometry of carbonatites as an indicator of diagenetic alteration. Geochimica et Cosmochimica Acta 74, 4110–4122.
Dennis, K.J., Affek, H.P., Passey, B.H., Schrag, D.P., Eiler, J.M., 2011. Defining an absolute reference frame for 'clumped' isotope studies of CO_2. Geochimica et Cosmochimica Acta 75, 7117–7131.
Eiler, J.M., 2007. "Clumped-isotope" geochemistry - the study of naturally-occurring, multiply-substituted isotopologues. Earth and Planetary Science Letters 262, 309–327.
Eiler, J.M., 2011. Paleoclimate reconstruction using carbonate clumped isotope thermometry. Quaternary Science Reviews 30, 3575–3588.
Epstein, S.A., Clark, D., 2009. Hydrocarbon potential of the Mesozoic carbonates of the Bahamas. Carbonates and Evaporites 24, 97–138.
Eren, M., Kaplan, M.Y., Kadür, S., 2007. Petrography, geochemistry and origin of Lower Liassic dolomites in the Aydnck area, Mersin, southern Turkey. Turkish Journal of Earth Sciences 16, 339–362.
Fan, T., Yu, K., Zhao, J., Jiang, W., Xu, S., Zhang, Y., Wang, R., Wang, Y., Feng, Y., Bian, L., 2020. Strontium isotope stratigraphy and paleomagnetic age constraints on the evolution history of coral reef islands, northern South China Sea. Geological Society of America Bulletin 132, 803–816.
Fedorov, A.V., Brierley, C.M., Lawrence, K.T., Liu, Z., Dekens, P.S., Ravelo, A.C., 2013. Patterns and mechanisms of early Pliocene warmth. Nature 496, 43–49.
Fritz, P., Smith, D., 1970. The isotopic composition of secondary dolomites. Geochimica et Cosmochimica Acta 34, 1161–1173.
Ghosh, P., Adkins, J., Affek, H., Balta, B., Guo, W.F., Schauble, E.A., Schrag, D., Eiler, J.M., 2006. ^{13}C—^{18}O bonds in carbonate minerals: a new kind of paleothermometer. Geochimica et Cosmochimica Acta 70, 1439–1456.
Guo, Y., Deng, W.F., Liu, X., Kong, K., Yan, W., Wei, G.J., 2021. Clumped isotope geochemistry of island carbonates in the South China Sea: implications for early diagenesis and dolomitization. Marine Geology 437, 106513. https://doi.org/10.1016/j.margeo.2021.106513.
Haq, B.U., Hardenbol, J., Vail, P.R., 1987. Chronology of fluctuating sea levels since the Triassic. Science 235, 1156–1167.
Hemingway, J.D., Henkes, G.A., 2021. A disordered kinetic model for clumped isotope bond reordering in carbonates. Earth and Planetary Science Letters 566, 116962. https://doi.org/10.1016/j.epsl.2021.116962.
Henkes, G.A., Passey, B.H., Grossman, E.L., Stanton, B.J., Perez-Huerta, A., Yancey, T.E., 2014. Temperature limits for preservation of primary calcite clumped isotope temperatures. Geochimica et Cosmochimica Acta 139, 362–382.
Henkes, G.A., Passey, B.H., Grossman, E.L., Shenton, B.J., Yancey, T.E., Perez-Huerta, A., 2018. Temperature evolution and the oxygen isotope composition of Phanerozoic oceans from carbonate clumped isotope thermometry. Earth and Planetary Science Letters 490, 40–50.
Herbert, T.D., Lawrence, K.T., Tzanova, A., Peterson, L.C., Caballero-Gill, R., Kelly, C.S., 2016. Late Miocene global cooling and the rise of modern ecosystems. Nature Geoscience 9, 843–847.
Horita, J., 2014. Oxygen and carbon isotope fractionation in the system dolomite–water–CO_2 to elevated temperatures. Geochimica et Cosmochimica Acta 129, 111–124.
Huntington, K.W., Budd, D.A., Wernicke, B.P., Eiler, J.M., 2011. Use of clumped-isotope thermometry to constrain the crystallization temperature of diagenetic calcite. Journal of Sedimentary Research 81, 656–669.
Jones, B., 2005. Dolomite crystal architecture: genetic implications for the origin of the Tertiary dolostones of the Cayman Islands. Journal of Sedimentary Research 75, 177–189.
Jones, B., 2007. Inside–out dolomite. Journal of Sedimentary Research 77, 539–551.
Jones, B., Hunter, I.G., 1994. Messinian (late Miocene) karst on Grand Cayman, British West Indies: an example of an erosional sequence boundary. Journal of Sedimentary Research 64, 531–541.
Jones, B., Luth, R.W., MacNeil, A.J., 2001. Powder X-ray diffraction analysis of homogeneous and heterogeneous sedimentary dolostones. Journal of Sedimentary Research 71, 790–799.
Kaufman, J., 1994. Numerical models of fluid flow in carbonate platforms: implications for dolomitization. Journal of Sedimentary Research 64, 128–139.
Kennett, J.P., Shackleton, N.J., 1975. Laurentide ice sheet meltwater recorded in Gulf of Mexico deep-sea cores. Science 188, 147–150.
Kim, S.T., Coplen, T.B., Horita, J., 2015. Normalization of stable isotope data for carbonate minerals: implementation of IUPAC guidelines. Geochimica et Cosmochimica Acta 158, 276–289.
Land, L.S., 1985. The origin of massive dolomite. Journal of Geological Education 33, 112–125.
Land, L.S., 1998. Failure to precipitate dolomite at 25°C from dilute solution despite 1000-fold oversaturation after 32 years. Aquatic Geochemistry 4, 361–368.
Lu, C., Murray, S., Koeshidayatullah, A., Swart, P.K., 2022. Clumped isotope acid fractionation factors for dolomite and calcite revisited: should we care? Chemical Geology 588, 120637. https://doi.org/10.1016/j.chemgeo.2021.120637.
Lukoczki, G., Haas, J., Gregg, J.M., Machel, H.G., Kele, S., John, C.M., 2020. Early dolomitization and partial burial recrystallization: a case study of Middle Triassic peritidal dolomites in the Villány Hills (SW Hungary) using petrography, carbon, oxygen, strontium and clumped isotope data. International Journal of Earth Sciences 109, 1051–1070.
Machel, H.G., 2004. Concepts and models of dolomitization: a critical reappraisal. In: Braithwaite, C.J.R., Rizzi, G., Darke, G. (Eds.), The Geometry and Petrogenesis of Dolomite Hydrocarbon ReservoirsGeological Society, London, Special Publicationsvol. 235, pp. 7–63.
Matthews, A., Katz, A., 1977. Oxygen isotope fractionation during the dolomitization of calcium carbonate. Geochimica et Cosmochimica Acta 41, 1431–1438.
Mcarthur, J.M., Howarth, R.J., Bailey, T.R., 2001. Strontium isotope stratigraphy: LOWESS Version 3: best fit to the marine Sr-isotope curve for 0–509 Ma and accompanying look-up table for deriving numerical age. Journal of Geology 109, 155–170.
McKenzie, J.A., Isern, A., Elderfield, H., Williams, A., Swart, P.K., 1993. Strontium isotope dating of paleoceanographic, lithologic, and dolomitization events on the northeastern Australian Margin, leg 133. In: McKenzie, J.A., Davies, P.J., Palmer Julson, A.A., Betzler, C.G., Brachert, T.C., Chen, M.-P.P., Crumiere, J.P., Dix, G.R., Droxler, A.W., Feary, D.A., Gartner, S., Glenn, C.R., Isern, A., Jackson, P.D., Jarrard, R.D., Katz, M.E., Konishi, K., Kroon, D., Ladd, J.W., Marin, J.M., McNeill, D.F., Montaggioni, L.F., Miiller, D.W., Omarzai, S.K., Pigram, C.J., Swart, P.K., Symonds, P.A., Watts, K.F., Wei, W. (Eds.), Proceedings Ocean Drilling Program. Scientific Resultsvol. 133, pp. 489–498.
Melim, L.A., Scholle, P.A., 2002. Dolomitization of the Capitan Formation forereef facies (Permian, West Texas and New Mexico): seepage reflux revisited. Sedimentology 49, 1207–1227.
Miller, K.G., Kominz, M.A., Browning, J.V., Wright, J.D., Mountain, G.S., Katz, M.E., Sugarman, P.J., Cramer, B.S., Christie-Blick, N., Pekar, S.F., 2005. The Phanerozoic record of global sea-level change. Science 310, 1293–1298.
Morrow, D., 1982a. Diagenesis 1. Dolomite-part 1: the chemistry of dolomitization and dolomite precipitation. Geoscience Canada 9, 5–13.
Morrow, D., 1982b. Diagenesis 2. Dolomite-part 2: dolomitization models and ancient dolostones. Geoscience Canada 9, 95–107.
Müller, I.A., Rodriguez-Blanco, J.D., Storck, J.C., do Nascimento, G.S., Bontognali, T.R.R., Vasconcelos, C., Benning, L.G., Bernasconi, S.M., 2019. Calibration of the oxygen and clumped isotope thermometers for (proto-) dolomite based on synthetic and natural carbonates. Chemical Geology 525, 1–17.
Murray, S.T., Swart, P.K., 2017. Evaluating formation fluid models and calibrations using clumped isotope paleothermometry on Bahamian dolomites. Geochimica et Cosmochimica Acta 206, 73–93.
Murray, S.T., Arienzo, M.M., Swart, P.K., 2016. Determining the Δ_{47} acid fractionation in dolomites. Geochimica et Cosmochimica Acta 174, 42–53.
Murray, S.T., Higgins, J.A., Holmden, C., Lu, C., Swart, P.K., 2021. Geochemical fingerprints of dolomitization in Bahamian carbonates: evidence from sulphur, calcium, magnesium and clumped isotopes. Sedimentology 68, 1–29.
Northrop, D.A., Clayton, R.N., 1966. Oxygen-isotope fractionations in systems containing dolomite. The Journal of Geology 74, 174–196.
Ohde, S., Elderfield, H., 1992. Strontium isotope stratigraphy of Kita-daito-jima Atoll, North Philippine Sea: implications for Neogene sea-level change and tectonic history. Earth and Planetary Science Letters 113, 473–486.
O'Neil, J.R., Epstein, S., 1966. Oxygen isotope fractionation in the system dolomite–calcite–carbon dioxide. Science 152, 198–201.
Pang, X., Chen, C.M., Shi, H.S., Shu, Y., Shao, L., He, M., Shen, J., 2005. Response between relative sea-level change and the Pearl River deep-water fan system in the South China Sea. Earth Science Frontiers 12, 167–177 (in Chinese with English abstract).
Passey, B.H., Henkes, G.A., 2012. Carbonate clumped isotope bond reordering and geospeedometry. Earth and Planetary Science Letters 351, 223–236.
Petersen, S.V., Defliese, W.F., Saenger, C., Daëron, M., Huntington, K.W., John, C.M., Winkelstern, I.Z., 2019. Effects of improved ^{17}O correction on interlaboratory agreement in clumped isotope calibrations, estimates of mineral-specific offsets, and temperature dependence of acid digestion fractionation. Geochemistry, Geophysics, Geosystems 20, 3495–3519.
Pigram, C., Davies, P., Feary, D., Symonds, P., 1992. Absolute magnitude of the second-order middle to late Miocene sea-level fall, Marion Plateau, northeast Australia. Geology 20, 858–862.
Qing, H., 1998. Petrography and geochemistry of early-stage, fine- and medium-crystalline dolomites in the Middle Devonian Presqu'ile Barrier at Pine Point, Canada. Sedimentology 45, 433–446.
Qing, H., Bosence, D.W.J., Rose, E.P.F., 2001. Dolomitization by penesaline sea water in Early Jurassic peritidal platform carbonates, Gibraltar, western Mediterranean. Sedimentology 48, 153–163.
Rameil, N., 2008. Early diagenetic dolomitization and dedolomitization of Late Jurassic and earliest Cretaceous platform carbonates: a case study from the Jura Mountains (NW Switzerland, E France). Sedimentary Geology 212, 70–85.
Ren, M., Jones, B., 2018. Genesis of island dolostones. Sedimentology 65, 2003–2033.
Rosenbaum, J., Sheppard, S., 1986. An isotopic study of siderites, dolomites and ankerites at high temperatures. Geochimica et Cosmochimica Acta 50, 1147–1150.
Roveri, M., Flecker, R., Krijgsman, W., Lofi, J., Lugli, S., Manzi, V., Sierro, F.J., Bertini, A., Camerlenghi, A., De Lange, G., Govers, R., Hilgen, F.J., HÅNubscher, C., Meijer, P.T., Stoica, M., 2014. The Messinian Salinity Crisis: past and future of a great challenge for marine sciences. Marine Geology 352, 25–58.
Saller, A.H., 1984. Petrologic and geochemical constraints on the origin of subsurface dolomite, Enewetak Atoll: an example of dolomitization by normalseawater. Geology 12, 217–220.
Schauble, E.A., Ghosh, P., Eiler, J.M., 2006. Preferential formation of ^{13}C—^{18}O bonds in carbonate minerals, estimated using first-principles lattice dynamics. Geochimica et Cosmochimica Acta 70, 2510–2529.
Shao, L., Li, Q., Zhu, W., Zhang, D., Qiao, P., Liu, X., You, L., Cui, Y., Dong, X., 2017a. Neogene carbonate platform development in the NW South China Sea: litho-, bio- and chemostratigraphic evidence. Marine Geology 385, 233–243.
Shao, L., Cui, Y., Qiao, P., Zhang, D., Liu, X., Zhang, C., 2017b. Sea-level changes and carbonate platform evolution of the Xisha Islands (South China Sea) since the Early Miocene. Palaeogeography Palaeoclimatology Palaeoecology 485, 504–516.
Sheppard, S.M., Schwarcz, H.P., 1970. Fractionation of carbon and oxygen isotopes and magnesium between coexisting metamorphic calcite and dolomite. Contributions to Mineralogy and Petrology 26, 161–198.

Simms, M., 1984. Dolomitization by groundwater–flow system in carbonate platforms. Transactions. Gulf Coast Association of Geological Societies 34, 411–420.
Stolper, D.A., Eiler, J.M., 2015. The kinetics of solid-state isotope-exchange reactions for clumped isotopes: a study of inorganic calcites and apatites from natural and experimental samples. American Journal of Science 315, 363–411.
Sun, S.Q., 1994. A reappraisal of dolomite abundance and occurrence in the Phanerozoic. Journal of Sedimentary Petrology 64, 396–404.
Tang, J., Dietzel, M., Fernandez, A., Tripati, A.K., Rosenheim, B.E., 2014. Evaluation of kinetic effects on clumped isotope fractionation (Δ_{47}) during inorganic calcite precipitation. Geochimica et Cosmochimica Acta 134, 120–136.
Thompson, P.R., Abbott, W.H., 2003. Chronostratigraphy and microfossil-derived sea-level history of the Qiongdongnan and Yinggehai basins, South China Sea. In: Olson, H.C., Leckie, R.M. (Eds.), Microfossils as Proxies of Sea-level Change and Stratigraphic Discontinuities. Society of Economic Paleontologists and Mineralogists, Special Publications, Tulsa, pp. 97–117.
Vail, P.R., Mitchum, R.M., 1979. Global cycles of relative changes of sea level from seismic stratigraphy: resources, comparative structure and eustatic changes in sea level. American Association of Petroleum Geologists Memoir 29, 469–472.
Vasconcelos, C., McKenzie, J.A., Warthmann, R., Bernasconi, S.M., 2005. Calibration of the $\delta^{18}O$ paleothermometer for dolomite precipitated in microbial cultures and natural environments. Geology 33, 317–320.
Veillard, C.M., John, C.M., Krevor, S., Najorka, J., 2019. Rock-buffered recrystallization of Marion Plateau dolomites at low temperature evidenced by clumped isotope thermometry and X-ray diffraction analysis. Geochimica et Cosmochimica Acta 252, 190–212.
Wang, R., Yu, K., Jones, B., Wang, Y., Zhao, J., Feng, Y., Bian, L., Xu, S., Fan, T., Jiang, W., Zhang, Y., 2018. Evolution and development of Miocene "island dolostones" on Xisha Islands, China South Sea. Marine Geology 406, 142–158.
Wang, R., Jones, B., Yu, K., 2019. Island dolostones: genesis by time-transgressive or event dolomitization. Sedimentary Geology 390, 15–30.
Wang, L., Shi, X., Ben, Z., Pei, J., Yang, X., Shen, Y., Shi, D., Liu, K., Zhao, P., Yan, A., 2020. Tectono-themal evolution features of the reef body developing area in the Liyue Basin, southern South China Sea. Chinese Journal of Geophysics 63, 3050–3062 (in Chinese with English abstract).
Wang, R., Yu, K., Jones, B., Jiang, W., Xu, S., Fan, T., Zhang, Y., 2021. Dolomitization microconditions constraint on dolomite stoichiometry: a case study from the Miocene Huangliu Formation, Xisha Islands, South China Sea. Marine and Petroleum Geology 133, 105286. https://doi.org/10.1016/j.marpetgeo.2021.105286.
Warren, J., 2000. Dolomite: occurrence, evolution and economically important associations. Earth-Science Reviews 52, 1–81.
Wei, K., Cui, H., Ye, S., Li, D., Liu, T., Liang, J., Yang, G., Wu, L., Zhou, X., Hao, Y., 2001. High-precision sequence stratigraphy in Qiongdongnan Basin. Earth Science - Journal of China University of Geosciences 26, 59–66 (in Chinese with English abstract).
Wheeler, C.W., Aharon, P., 1997. The geology and hydrogeology of Niue, South Pacific. In: Vacher, H.L., Quinn, T.M. (Eds.), Geology and Hydrology of Carbonate Islands. Developments in Sedimentology. Elsevier, Amsterdam, pp. 537–564.
Whitaker, R.E., Smart, E.L., Jones, G., 2004. Dolomitization: from conceptual to numerical models. In: Braithwaite, C.J.R., Rizzi, G., Darke, G. (Eds.), The Geometry and Petrogenesis of Dolomite Hydrocarbon Reservoirs. Geological Society, London, Special Publicationsvol. 235, pp. 99–139.
Winkelstern, I.Z., Lohmann, K.C., 2016. Shallow burial alteration of dolomite and limestone clumped isotope geochemistry. Geology 44, 467–470.
Winkelstern, I.Z., Kaczmarek, S.E., Lohmann, K.C., Humphrey, J.D., 2016. Calibration of dolomite clumped isotope thermometry. Chemical Geology 443, 32–38.
Wu, S., Yang, Z., Wang, D., Lü, F., Lüdmann, T., Fulthorpe, C., Wang, B., 2014. Architecture, development and geological control of the Xisha carbonate platforms, northwestern South China Sea. Marine Geology 350, 71–83.
Yi, L., Jian, Z., Liu, X., Zhu, Y., Zhang, D., Wang, Z., Deng, C., 2018. Astronomical tuning and magneto-stratigraphy of Neogene biogenic reefs in Xisha Islands: South China Sea. Science Bulletin 63, 564–573.
Zaarur, S., Affek, H.P., Brandon, M.T., 2013. A revised calibration of the clumped isotope thermometer. Earth and Planetary Science Letters 382, 47–57.
Zachos, J., Pagani, M., Sloan, L., Thomas, E., Billups, K., 2001. Trends, rhythms, and aberrations in global climate 65 Ma to present. Science 292, 686–693.
Zhang, M.S., He, Q.X., Ye, Z.J., 1989. The Geologic Research of Deposition of Bioherm Carbonate in the Xisha Islands. Science Press, Beijing (30 pp.).
Zhang, Y., Pagani, M., Liu, Z., 2014. A 12-million-year temperature history of the tropical Pacific Ocean. Science 344, 84–87.
Zhang, Y., Yu, K., Qian, H., Fan, T., Yue, Y., Wang, R., Jiang, W., Xu, S., Wang, Y., 2020. The basement and volcanic activities of the Xisha Islands: evidence from the kilometre-scale drilling in the northwestern South China Sea. Geological Journal 55, 571–583.
Zhao, Q., 2010. The Sedimentary Research About Reef Carbonate in Xisha Islands Waters. Institute of Oceanology, Chinese Academy of Sciences, Qingdao (Ph.D. thesis, 158 pp.).
Zhao, H., Jones, B., 2012. Origin of "island dolostones": a case study from the Cayman Formation (Miocene), Cayman Brac, British West Indies. Sedimentary Geology 243, 191–206.
Zheng, Y.F., 1999. Oxygen isotope fractionation in carbonate and sulfate minerals. Geochemical Journal 33, 109–126.
Zhu, W., Xie, X., Wang, Z., Zhang, D., Zhang, C., Cao, L., Shao, L., 2017. New insights on the origin of the basement of the Xisha Uplift, South China Sea. Science China Earth Sciences 60, 2214–2222 (in Chinese with English abstract).